Analysis of electrode deformations in deep brain stimulation surgery.

Florent Lalys, Claire Haegelen, Tiziano d'Albis, Pierre Jannin

Analysis of electrode deformations in Deep Brain Stimulation surgery

Florent Lalys [1,2] , Claire Haegelen [1,2,3] , Tiziano D'Albis [1,2] , Pierre Jannin [1,2]

[1] INSERM, U1099, Rennes, F-35000, France
[2] University of Rennes 1, LTSI, Rennes, F-35000, France
[3] CHU Rennes, Department of Neurosurgery, Rennes, F-35000, France

Abstract

Purpose: Deep Brain Stimulation (DBS) surgery is used to reduce motor symptoms when movement disorders are refractory to medical treatment. Postoperative brain morphology can induce electrode deformations as the brain recovers from an intervention. The inverse brain shift has a direct impact on accuracy of the targeting stage, so analysis of electrode deformations is needed to predict final positions.

Methods: DBS electrode curvature was evaluated in 76 adults with movement disorders who underwent bilateral stimulation and the key variables that affect electrode deformations were identified. Non-linear modelling of the electrode axis was performed using post-operative Computed Tomography (CT) images. A mean curvature index was estimated for each patient electrode. Multivariate analysis was performed using a regression decision tree to create a hierarchy of predictive variables. The identification and classification of key variables that determine electrode curvature were validated with statistical analysis.

Results: The principal variables affecting electrode deformations were found to be the date of the post-operative CT scan and the stimulation target location. The main pathology, patient's gender, and disease duration had a smaller although important impact on brain shift.

Conclusions: The principal determinants of electrode location accuracy during DBS procedures were identified and validated. These results may be useful for improved electrode targeting with the help of mathematical models.

Keywords: Deep Brain Stimulation, electrode curvature, targeting accuracy, brain-shift

1. Introduction

1.1. Context

Deep Brain Stimulation (DBS) is currently the most favoured treatment of patients with motor disorders such as Parkinson's Disease (PD), tremor or dystonia whose symptoms do not respond to medical therapy [1]. Recently, it has also shown impressive results on patients with severe neurological disorders such as Tourette syndrome [2] or major depression [3]. For now, the three major targets according to the patients' diseases are the caudal part of the ventro-lateral thalamic nucleus, the medial Globus Pallidus (GPm) and the Sub-Thalamic Nucleus (STN). In spite of its effectiveness, DBS also presents several limitations, e.g., it can cause several types of neuropsychological disorders [4-7]. As a consequence, the accuracy of electrode placement is crucial to avoid unwanted stimulation of non-target brain areas. As DBS surgery is a standard stereotactic procedure, one source of inaccuracy is due to brain-shift phenomenon, occurring during [8-10] and after DBS surgery [11]. The impact of brain shift on the accuracy of electrode placement is considerable and has motivated extended research on new surgical techniques on one hand, and on a better understanding, modelling and anticipation of brain-shift phenomena on the other hand. Brain-shift during DBS surgery can be decomposed into two main phenomena: the intra-operative and the post-operative brain shift. During surgery, after the opening of the dura mater, a brain-shift may occur due to the loss of Cerebrospinal Fluid (CSF) and the intra-cranial invasion of subdural air. Several days after the procedure, a post-operative displacement may appear, when the subdural air resolves and the brain returns to its initial position. This second phenomenon is known as the inverse or reversal of the intra-operative brain shift.

1.2. Related works

As brain-shift has a negative impact on the accuracy of DBS surgery, an alternative but more intuitive approach to the analysis of phenomena is the development of surgical techniques to counteract this phenomenon [10,12]. However, brain-shift results remains non-negligible in some case and some neurosurgery departments still have some important issues. For anticipating intra-operative brain shift, lots of work has been done on soft tissue deformation modelling for standard neurosurgical procedures [13,14]. Complex biomechanical models have also been proposed [15-17] focusing on the intra-operative craniotomy-induced brain-shift. Among these studies, however, only a few focused on DBS surgery. Pallavaran et al. [18,19] used somatotopy recordings and stimulation responses to demonstrate the presence of brain-shift in DBS. Later, Bilger et al. [20] proposed a biomechanical model of brain-shift in DBS surgery taking into account post-operative phenomena.

To evaluate the inverse brain shift in DBS, several research works focused on the identification of the shift direction and on the quantification of electrode displacements. Miyagi et al. [21] studied both unilateral and bilateral implantations and concluded on the brain shift tendency for both type of procedures. Similarly, Halpern et al. [22] evaluated pre and post-operative MRI of patients who underwent STN DBS and concluded that the shift was posteriorly when patients were implanted in the supine position. Khan et al. [23] reported brain shifts up to 4mm in magnitude in the direction of gravity. Sillay et al. [11] also showed that the inverse brain shift had important consequences on electrode positions. Significant shift was identified along rostral, anterior and medial directions, with a greater shift found along the rostral direction (average of 1.41mm). Kim et al. [24] compared electrode positions estimated from the immediate post-operative CT (STN DBS surgery) with those estimated 6 months after surgery, and found significant displacement (0.6mm, 1.0mm and 1.0mm for the x, y and z-axis respectively). Similarly, van den Munckhof et al. [25] analysed postoperative electrode displacements by comparing CT scans taken immediately after surgery with CT scans taken after longer follow-up periods for 14 patients. By means of volumetric measurements, they found that the electrode displacement significantly correlated with the amount of subdural air found post-operatively, and that electrodes moved on average 3.3mm upward along the trajectory. In summary, these studies suggest that the brain happens mainly posteriorly with respect to the gravity, that the amount of shift is proportional to the amount of CSF leakage and that, for surgeons who don't use new proposed surgical techniques, the displacement of electrodes due to the brain-shift is non-negligible.

All these works were interesting in evaluating brain shift in DBS mainly by quantifying the volume of post-surgical intracranial air, but they did not propose any explanation or model of the phenomenon. Towards the identification of predictive factors affecting brain-shift in DBS, Obuchi et al. [26] observed that the width of the third ventricle remains the most reliable factor for predicting the brain-shift in STN-DBS. Other factors were also tested, such as patient's age, surgery duration, or bicaudate index, but were found having no impact on brain shift. Additionally, Azmi et al. [27] found a correlation between the accumulated volume of intracranial air and the degree of cerebral atrophy. Based on these results, as the degree of CSF loss is directly linked to the degree of intracranial air invasion, new studies have been proposed. Nazzarro et al. [28] identified factors such as brain atrophy, patient position or size of CSF space opening that directly affect the degree of CSF loss in DBS.

Similarly, in Slotty et al. [29], no significant correlation was found between volume of intracranial air and duration of surgery, as well as no significant difference on electrode deviations between the first and second side of surgery for bilateral implantations. On the contrary, Azmi et al. [27] found a greater error in stereotactic accuracy on the second side of the surgery.

Finally, little has been reported in the literature on the issue regarding the positions and curvatures of electrodes after DBS. Moreover, the identification of predictive factors that have an impact on these phenomena remains a difficult task. In this context, the objective of this paper was to identify a set of predictive variables that have an impact on the degree of brain-shift after surgery. For this purpose, in spite of evaluating the volume of air invasion within the brain, we were interested in quantifying the degree of curvature of electrodes, which is probably directly linked to the degree of brain shift. We applied a multi-variate analysis using a regression decision tree to create a hierarchy of predictive variables. Statistical analysis then validated this classification for the identification of key variables. Based on this hierarchy of predictive variables, we finally studied the curvature difference between electrode subsections in order to better understand and anticipate brain shift in DBS.

2. Materials and Methods

After introducing the data used in this study (Subsection 2.1), we propose an algorithm for automatic electrode segmentation. We estimated the electrode axis with a non-linear model (Subsection 2.2) and estimated a value corresponding to the degree of deformation of the electrode (Subsection 2.3), i.e. the curvature index. Then, we identified a set of predictive variables in Subsection 2.4. that allows a clustering of the electrodes into subgroups of similar curvature index. For this purpose, we applied a multi-variate analysis trough a regression decision tree. In order to validate the impact of these variables on electrode curvatures, we then performed statistical comparisons (Subsection 2.5). Finally, based on the predictive variables previously identified, we investigated local curvatures by defining three spatial sections along the electrode length (Subsection 2.6).

2.1. Data-set

Our data-set consisted of 76 patients who had undergone bilateral STN or GPm DBS surgeries selected according to strict inclusion criteria [30-32]. Patient pathologies were mostly PD [30] with a mixed, tremor or akinesia form, but also Dystonia and Tourette syndrome. The surgical procedure was performed under local anaesthesia, and the target location estimated during the planning is implemented with a stereotactic frame. During the intervention, an X-ray control was performed as well as electrophysiological explorations and clinical tests. Single track microelectrode recording was performed for each electrode. For each patient, both a pre operative 3T T1-weighted MR image (1mm x 1mm x 1mm, Philips Medical system) and a post-operative CT scan image (0.44 mm x 0.44 mm x 0.6 mm, GE Healthcare VCT 64) were performed. All CT and MR images were pre-processed with a non-local means denoising algorithm [33]. During the surgery, patients were implanted in supine position. The study was approved by the local research ethics committee, and informed consent was obtained from all participants.

2.2. Electrode curve modelling

To estimate the trajectories of the implanted electrodes, we developed an automatic algorithm based on the segmentation of the electrode axis from post-operative Computed Tomography (CT) images. First, the post-operative CT scan was linearly registered to the MR images with an affine transformation (algorithm: Newuoa, cost function: normalized mutual information, interpolation: Spline3) [34], where the brain mask, Anterior Commissure (AC) and Posterior Commissure (PC) were previously extracted using the BrainVisa® (*http://brainvisa.info/)* software. After reformating, we segmented the hyper-signal artefacts generated by the electrodes by thresholding the registered CT volume within the region identified by the brain mask. This segmentation allowed us to determine the centres of each hyper-signal region for each slice. Connected components were then applied and the two largest point clouds were kept, corresponding to the two electrode point clouds. We finally applied a non-linear regression [35] to fit both point clouds to a polynomial function. Non-linear regression is used to relate a response to a vector of predictor variables, where the prediction equation depends nonlinearly on one or more unknown parameters. In order to determine the best degree of the polynomial curve, we performed a manual segmentation of the electrode axis for 20 patients and compared all point clouds with the curve fitting of the modelling. The method presented here may also be helpful to extract the coordinates of electrodes contacts, given the geometry of the electrode model [36].

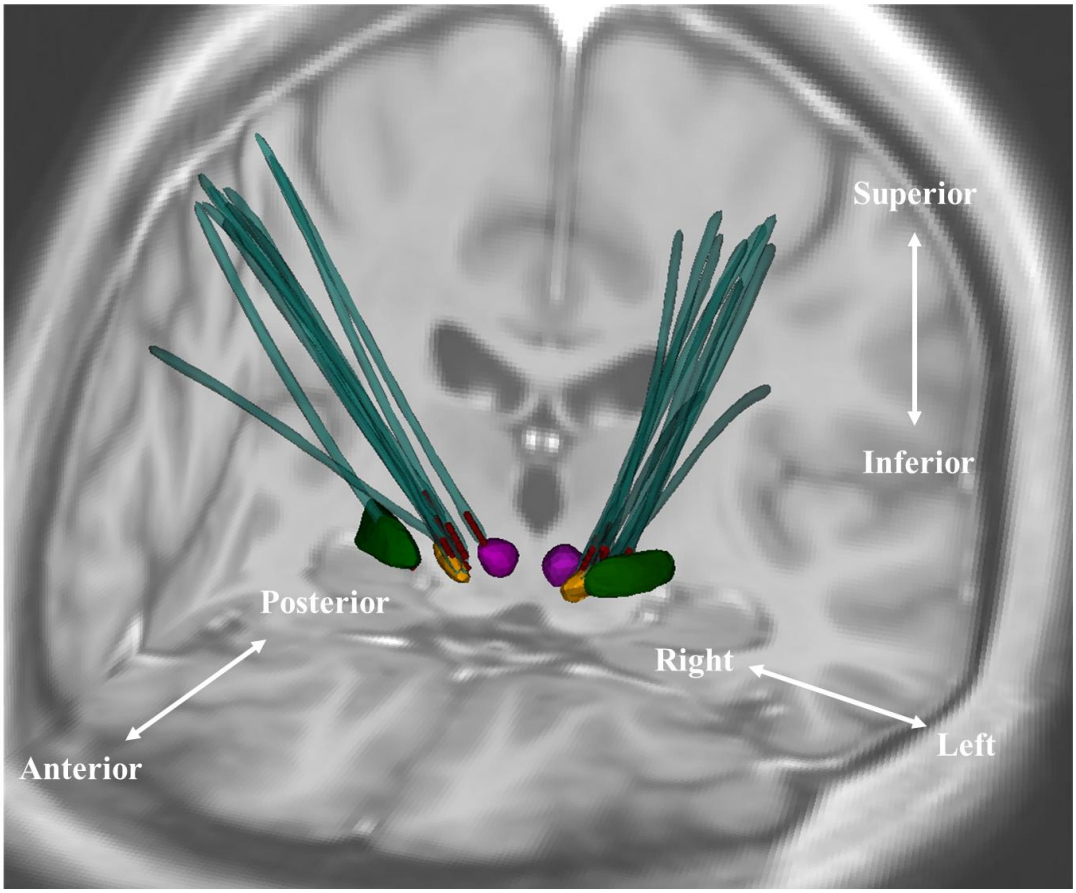

Figure 1. 20 segmented electrodes from 10 STN DBS patients warped into a template. In red: segmented contacts. Structures: Green: GPm, Yellow: STN, pink: red nucleus.

2.3. Extraction of curvature index

A parametrical definition of the fitted curve was obtained: $\vec{r}(n) = (x(n), y(n), z(n))$. We computed an index corresponding to the mean degree of curvature along the electrode axis [37] as follows. The curvature was defined as the inverse of the radius of curvature. In 2D, given a point belonging to a curve, there is a unique circle or line, which most closely approximates the curve at that point. In 3D, and given the parametrically defined space curve, a local expression of the curvature (i.e. Local Curvature Index, LCI) is given by:

$$LCI = \frac{\sqrt{(z''y' - y''z')^2 + (x''z' - z''x')^2 + (y''x' - x''y')^2}}{(x'^2 + y'^2 + z'^2)^{3/2}}$$

In order to compute the Mean Curvature Index (MCI) of a curve, the local expression of the curvature is averaged over the entire electrode length:

$$MCI = \frac{1}{N}\sum_{n=1}^{N} LCI(n)$$

with N the number of voxels used for the electrode point cloud. The MCI value is a non-unit value.

Using the equation of the LCI, another index could be easily computed: the maximum curvature index. In order to test the correlation between both indexes, they were extracted and statistically compared for each electrode using the independence Pearson Chi-squared test. Both indexes were found dependent (p=0.02), and we decided to keep the MCI for the rest of the study.

2.4. Multi-variate analysis

In order to cluster the electrodes according to MCI similarity, and toward the objective of identifying predictive variables that play a role into the degree of electrode curvature, we applied a multi-variate analysis. In our analysis, the MCI is the variable that has to be explained by the others. A set of initial variables was therefore chosen, in accordance with the literature and some hypothesis expressed by neurosurgeons. Eight predictive variables were identified: order of electrode implantation, post-operative acquisition time of the CT scan, patient age, sex, primary pathology, form of the disease (i.e. the secondary pathology), stimulation target, and disease duration. The post-operative CT acquisition time, the age and the disease duration were quantitative variables, whereas all others were categorical. The male-to-female ratio of the patients was 36-40 with a mean age of 59.2 ± 7.6 years (range, 33~78). Half of the patients underwent bilateral STN DBS (38), and the other half of them bilateral GPm DBS. Only patients with bilateral implantation were selected in order to keep a homogeneous data-set and avoid local brain shift phenomena that can be present on unilateral implantations. As only bilateral implantations were chosen, we had the same number of electrodes implanted in first and second position (76 for each). Fig 2. illustrates the distribution along with their range of the 4 other variables: CT scan delay, the disease duration, the main and secondary pathology. Some of these variables seemed to be not independent, e.g. the main pathology associated with the form of the pathology is often linked to the stimulation target chosen by surgeons. In order to test for independency, we performed the independence Pearson Chi-squared test between each variable pair (with a 0.05 significance level).

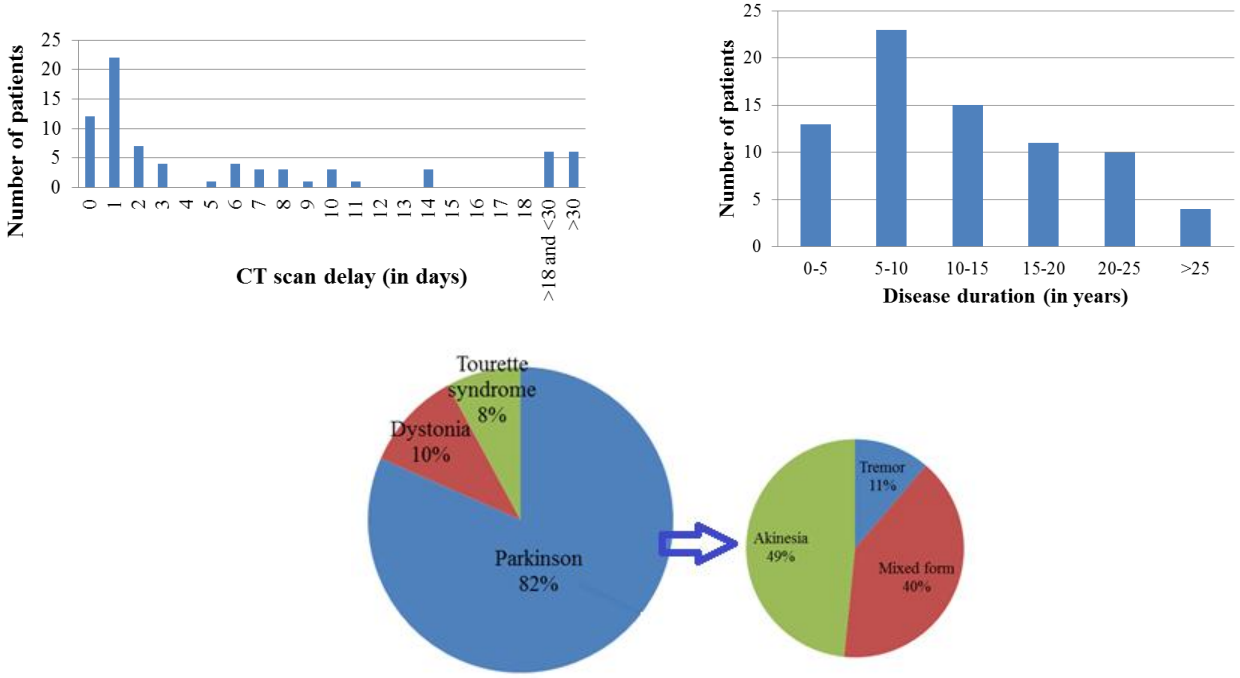

Figure 2. Distributions of predictive variables: Above: post-operative delay of the CT acquisition. Middle: disease duration. Below: Main pathology (left) and form of the disease (right) only for Parkinsonian patients.

As predictive variables were both quantitative and categorical, we chose to use the regression decision tree with the CART algorithm and Gini criterion [38]. The minimum number of observations per leaf node was fixed to 10 in order to keep enough electrodes in each subgroup to test for statistical significance. The objective of this algorithm is to identify explaining variables in their order of importance. Regression decision tree was therefore chosen to estimate the impact of the 8 variables on the degree of electrode curvature. As a result, we obtained a hierarchy of predictive variables that cluster electrodes with similar MCIs.

2.5. Statistical analysis

Once electrodes have been clustered according to results of the regression decision tree, statistical comparisons were performed between the identified clusters. As results showed a non-parametric distribution, the Mann-Whitney U-test was used for comparison between electrodes clusters. A p-value of less than 0.05 was deemed significant in the analysis.

2.6. Subdivision of electrodes into spatial sections

To better comprehend the electrode curvature phenomenon, and instead of estimating only one MCI for the entire electrode axis, we defined three spatial sections along the electrode length and estimated one MCI per section. After the registration of the CT scan to the MRI of the patient, and knowing the position of AC and PC on the patient MRI, we defined three zones in the AC-PC coordinate space. The upper zone was defined from 25mm above the AC-PC line, and corresponds to the cortex zone. The second zone was defined between 25mm and 10mm above AC-PC and corresponds to the ventricles zone. Finally, the third zone was defined between 10mm above AC-PC and the tip of the electrodes (in the case of STN target, around 5mm below AC-PC), and is situated within the basal ganglia zone. Fig. 3. shows an example of such a subdivision on an average MR template built from an image data-set of Parkinsonian patients [39].

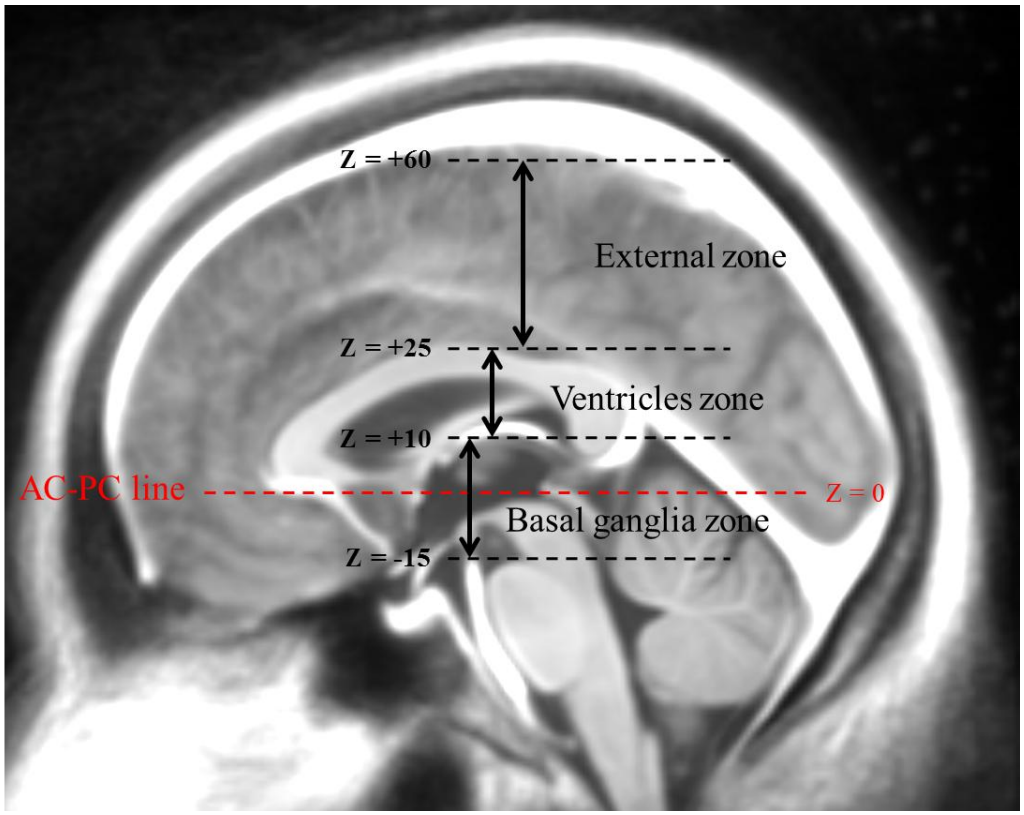

Figure 3. Subdivision of MRI in three zones according to AC-PC coordinates.

By means of this subdivision, a better description of the electrode curvature could be obtained. We identified four subgroups of patients based on the result of the decision tree. Creating four subgroups is equivalent to pruning the tree at the second level. With this pre-classification, it allows us to have homogeneous groups of patients while keeping at least 30 electrodes per subgroup.

3. Results

3.1. Curve modelling

A total of 152 electrodes from 76 patients were modelled. Results of the curve modelling (Tab. 1.) indicated that the higher the degree of the polynomial equation was, the better the modelling was. However, a high degree could also modify the real aspect of the electrode. Observing small error differences between the third and fourth degrees, we decided to keep a degree of 3 for the characteristic polynomial.

Characteristic polynomial	Mean electrode modelling error (std)
1st degree	0.27 (0.38)
2nd degree	0.17 (0.26)
3rd degree	0.10 (0.14)
4th degree	0.09 (0.12)

Table 1. Electrode modelling error using different degrees of characteristic polynomial.

The quality of the electrode segmentation could be directly linked to the results of the electrode curve modelling. However, we could easily imagine that even with segmentation errors, the impact on the final curve would be negligible as the curve is derived from a consequent points cloud. Moreover, errors found for the non-linear regression were very low (~0.1mm), and it allowed us to accurately extract curvature index.

3.2. Regression decision tree

Each variable was found to be independent to each other. Fig. 4. shows the regression decision tree computed from 152 electrodes modelled in our study. From the set of height predictive variables originally considered, three of them were completely excluded from the decision tree by the regression algorithm, i.e. the age, the order of the electrode and the pathology form. On the contrary, the CT scan delay resulted to be very important for the explanation of the MCI, as it appeared at the root level and then multiple times all along the tree. Similarly, stimulation target, patient sex, main pathology and disease duration resulted to have an impact on the MCI of electrodes after surgery.

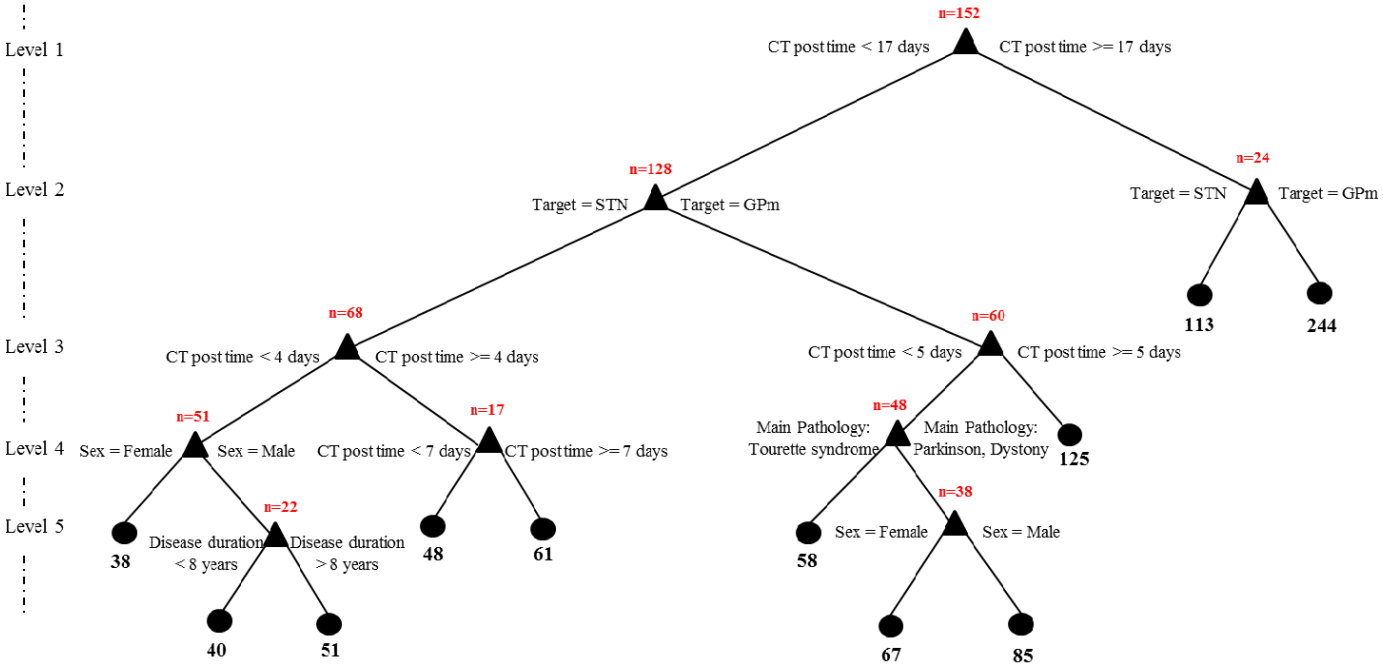

Figure 4. Regression decision tree, with the number of electrodes used at each parent node and the mean MCI calculated at each leaf node.

In order to study the evolution of the MCI according to the CT scan delay, we also computed MCIs for different subgroups of patients (Fig. 5.). For creating the different subgroups of patients, the cut-off values from the CT scan delay variables were used.

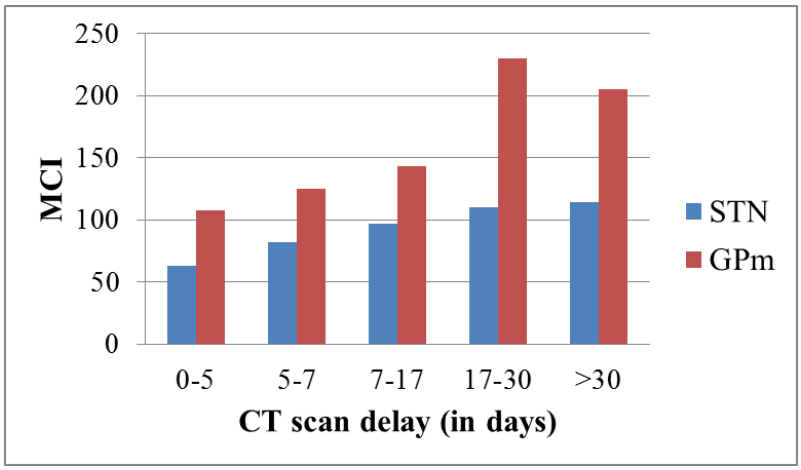

Figure 5. MCI evolution for the subgroup of STN patients and the subgroup of GPm patients.

3.3. Statistical comparisons

First, and in order to validate the hierarchy of predictive variables resulted from the regression algorithm, we defined cluster of electrodes based only on single variables and performed same statistical comparisons. For the three binary variables (sex, target, and order of implantation), we observed no significant MCI differences. For the two categorical variables "main pathology" and "disease form" (having both cardinality equal to three), we performed a multiple comparison test that also showed no differences between MCIs. For the three quantitative variables, it was impossible to determine separation values and it would not have made sense to set random values for this test. As no variable was easily identifiable to explain the differences between MCI values, the use of a decision tree and the creation of a hierarchy of predictive variables seemed to be very relevant. Complete results of statistical comparisons are shown on Fig. 6. The idea was to go down through the different levels of the tree and, at each node, to validate the clusters recursively defined with a statistical test.

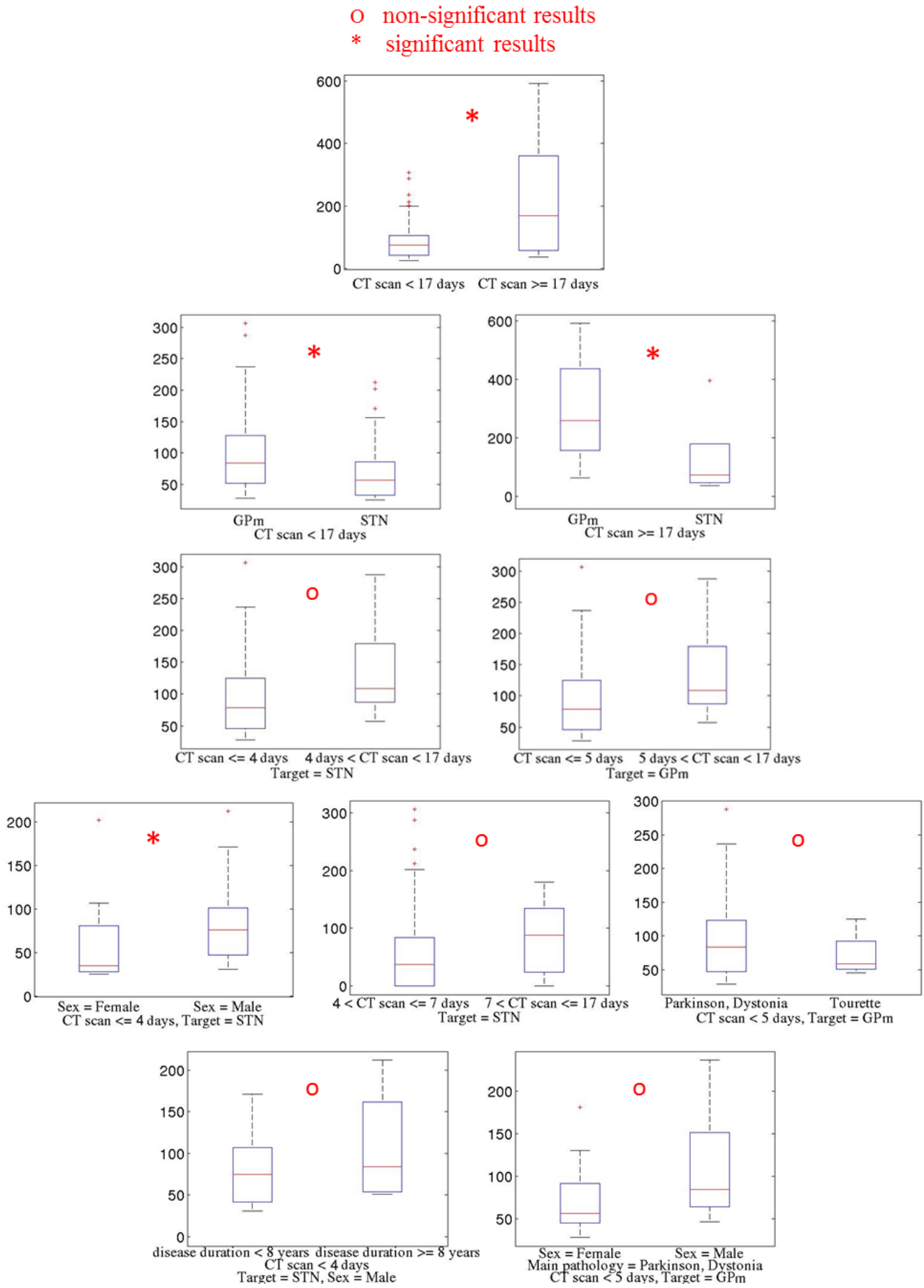

Figure 6. Statistical comparisons performed using results of the regression decision tree (one line per level). The y axis represents the MCI of electrodes.

At the root node, the primary and therefore most discriminant predictive variable affecting the MCI was the date of the CT scan, separating electrodes into two distinct groups: CT scans acquired before and after 17 days (p-value = 0.01), with a significant larger MCI for the second group.

At the second level, patients stimulated in the GPm showed larger MCI than patients stimulated in the STN for both nodes. The p-value was close to zero (p-value = 0.01) for patients having their CT scan performed less than 17 days after surgery, and equal to 0 for patients having their CT scan performed more than 17 days after surgery. For the first subgroup, many variables were then affecting the MCI. For the second one, MCIs were probably too close to each other to be further separated by any other variables. Therefore, for the rest of the tree, we were interested in the first group (left side of the tree), composed of 128 electrodes, with a CT scan delay inferior to 17 days.

At the third level, for patients who underwent STN DBS surgery, the CT scan delay appears again with a cut-off value equal to four days. However, this subdivision was not significant (p-value = 0.16). Interestingly, the same variable was also chosen for patients who underwent GPm DBS surgery, with sensibly the same cut-off value (five days), but as in the previous case the separation was not significant (p-value = 0.11).

At the fourth level, for STN patients with a CT scan acquired less than four days after surgery, female patients showed lower MCI than male patients (p-value=0.01). Additionally, for STN patients, two clusters were emerging: patients with a CT scan acquired between 4 and 7 days and patients with a CT scan acquired between 7 and 17 days (p-value=0.32) after the surgery. For GPm patients with a CT scan delay inferior to 5 days, the subgroup of patients suffering from Tourette syndrome showed lower MCI than the second subgroup of patients suffering from Parkinson or Dystonia disease (p-value = 0.55).

At the fifth level, for STN male patients having their CT scan acquired less than 4 days after surgery, the subgroup of patients who started to have motor symptoms earlier (with a cut-off value set to 8 years) showed lower MCI than the other (p-value = 0.4). Finally, for patients implanted within the GPm and suffering from Parkinson or dystonia symptoms, with a CT scan delay inferior to 5 days, the subgroup of female patients showed non-significant lower MCI than male patients (p-value=0.11).

3.4. Electrode section separation

Results of the local curvature analysis are shown on Fig. 7. No statistical differences (with significance level of 0.05) were found within each subgroup. However, general tendencies on the average and the variance within and between each subgroup have been found.

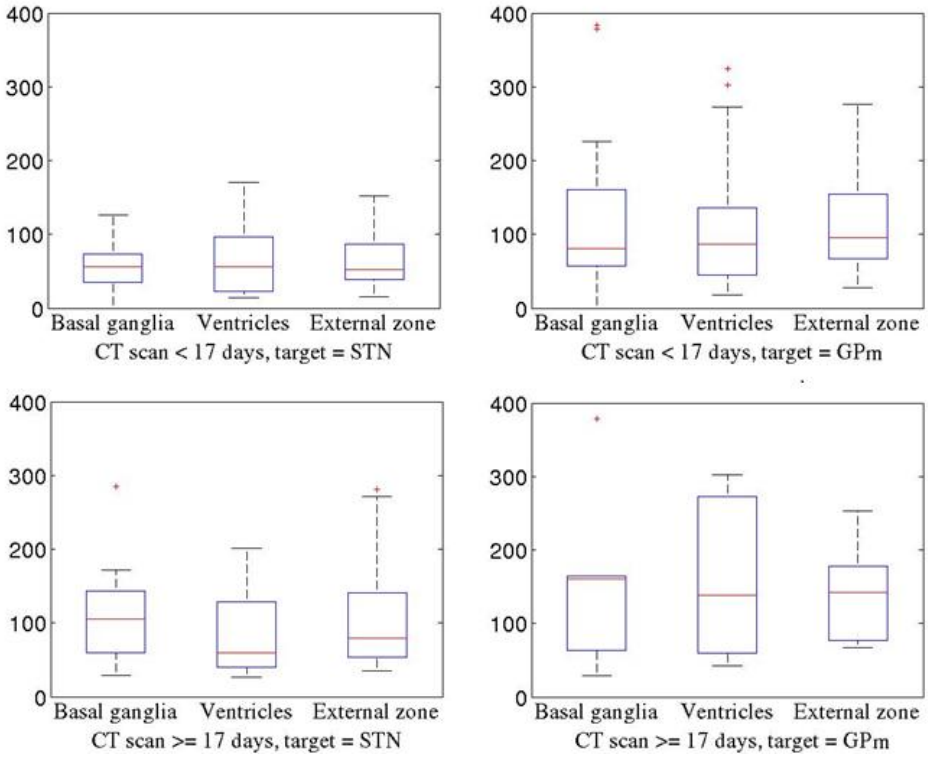

Figure 7. Statistical comparisons per electrode zones, given the predictive variables of level 2 of the tree. The y axis represents the MCI of electrodes.

4. Discussion

This study, based on the analysis of electrodes curvatures for a dataset of 76 patients, showed that the degree of brain shift was correlated with several key variables that have to be taken into account for further modelling in DBS surgeries. The results presented here aim to reach a higher degree of understanding of the brain shift phenomenon in DBS through the analysis of electrode curvature. We can easily imagine that a strong relation exists between the degree of electrode curvature and the degree of inverse brain shift, however this relation has not been demonstrated in the literature yet. Moreover, this work aimed at identifying key variables affecting electrode curvature during DBS surgery. In that sense, it is a first step towards the creation of mathematical models for the prediction of the degree of electrodes curvatures. In order to be able to create such mathematical models, however, a larger number of patients is required, as well as a larger number of potential affecting variables. A bigger data-set would for instance allow identifying precise variables distribution and creating linear or non-linear multivariate regression for explaining electrode curvature.

4.1. Primary predictive variables

Two predictive variables were found to be key variables affecting electrode curvature in DBS: the date of the CT scan and the stimulated target. The number of days passed between the surgery and the CT acquisition has been shown to be the predictive variable with the most impact on electrode MCI. Indeed, this variable is chosen at the root node of the decision tree and is present multiple times all along the tree. For this variable, different cut-off values resulted to be relevant in the decision tree: cut-off = 5, 7 and 17 days, showing the relative importance of this variable over the other. The different cut-off values also showed that the MCI is significantly increasing in the first two weeks, but seems to stabilize afterwards, since no other separation was proposed after the cut-off of 17 days (Fig. 5.). To validate this result, we compared MCI values for each leaf node at the right side of the tree (i.e. CT date > 17 days), with one subgroup of patients having their CT scan acquired between 2 weeks and 1 month after surgery, and one subgroup with patients having their CT scan acquired more than 1 month after surgery. The MCI values were found non-significant for both stimulation targets. Kim et al. [24] concluded their paper by an open question on the time to wait before evaluating the final position of electrodes in CT scans. Indeed, postoperative monitoring of the electrode position remains vital towards the assessment of the best stimulation site in DBS. In their work, they found no significant discrepancy of the centre of electrodes estimated in the brain CT scans acquired between 1 and 3 months after surgery. Based on our results, we recommend estimating the DBS electrode position in the brain from CT scans acquired at least 2 weeks after surgery when the potential inverse brain shift had resolved. With this result in this group of patients, we have proven that CSF loss and delayed brain re-expansion was a major factor in electrode curvature.

The targeted anatomical structure to be stimulated was also identified as a relevant predictive variable in our study. This variable, present at the second level of our decision tree, allowed us to identify clusters with similar MCI with statistical significance. This can be explained by the fact that GPm-DBS patients may suffer from a higher degree of cerebral atrophy than STN-DBS patients. As already shown in the literature, there is a correlation between the accumulated volume of intracranial air and the degree of cerebral atrophy [27]. Our GPm implanted patients, mostly parkinsonian patients with akinesia, may have a greater cerebral atrophy than patients implanted in the STN. This finding is in agreement with the results of Obuchi et al. [26] who demonstrated that the size of the third ventricle is a predictive factor for estimating the brain shift. The second explanation is related to the anatomical location of the target. The GPm, located more laterally than the STN, is more affected by the inverse brain-shift than deep structures close to the mid-sagittal line, leading to larger anatomical deformations and therefore larger electrode deformations.

4.2. Secondary predictive variables

The main pathology and the disease duration appear once within the decision tree, and seem therefore to have an impact, even minimal, on the electrode MCI. At the fifth level of the tree, patients with shorter disease duration (< 8 years) had lower MCI values than others. As cerebral atrophy is linked to the duration of the disease, the result is not surprising. Moreover, at the fourth level of the tree, patients with Parkinson and Dystonia pathologies had larger MCI values than patients with Tourette syndrome. This result is also not surprising, as patients with Tourette syndrome were all young or medium-age patients with no particular medical history, whereas patients with Parkinson's or Dystonia's disease were older patients easily subjected to cerebral atrophy.

The sex of the patient resulted to have non-negligible impact on the degree of brain shift, as it appears twice in the tree. One explanation could be that the MCI depends on the cerebral density. The higher the cerebral density, the greater the brain shift is. As the cerebral density could be lower in female than male patients, this could explain why electrode MCIs of female patients have been found to be lower than in male patients. However, further studies including the measure of cerebral density are required to reach a better understanding of this complex phenomenon.

4.3. Other predictive variables

The patient age has been found to have no impact. However, it remains linked to disease duration and the main pathology, even if both variables were found independent. The algorithm used for the creation of the tree found that both the patient main pathology and the disease duration were more discriminant than the patient age, explaining the fact that this variable didn't appear in any tree nodes. The second pathology has not surprisingly been found to have no impact. Even if we tested the independence of each variable pair, the target is often linked to the association of two variables: the main pathology and its form. As both variables already appeared upper in the tree, the form of the pathology turns out to have no impact. Finally, the order of implantation of the electrodes did not show any impact on the MCI. This result follows the conclusion of Slotty et al. [29] who found no significant difference on electrode deviations between the first and second side of surgery. This may be surprising, considering that the first dura matter incision causes a unilateral air invasion that is expected to be higher than the second dura matter incision. For instance, it was shown that errors in stereotactic accuracy due to intracranial air are more present on the second side [27]. According to our results, we can imagine that the intra operative brain shift is minimal compared to the post-operative brain shift that we model, when the brain returns to its initial position.

4.4. Local curvature analysis

Through an analysis of the electrode local curvature in three pre-defined zones, we observed that within each subgroup of electrodes identified by the regression algorithm, the three local MCI means were almost identical, even if the variance varied from zone to zone. This means that the curvature was approximately equally distributed on the entire length of electrodes. This is a very important result with respect to the idea of introducing non-linear electrode trajectories for DBS. Currently, the exact positioning of the electrode is usually planned assuming that the electrode trajectory is linear, but some companies have recently proposed the use of non-linear trajectories to anticipate and compensate the brain shift phenomenon. Despite its originality, this procedure would require a good comprehension of brain shift phenomena, especially regarding results on local electrode curvatures presented in this paper.

Additionally, we observed that the MCI variance for STN patients with a CT scan acquired earlier than 17 days after the surgery was very small. In these cases, implanted electrodes maintained an approximately linear trajectory as the subdural air had not completely resolved. On the contrary, GPm patients with a CT scan acquired earlier than 17 days after the surgery had already a higher variability, probably due to a higher degree of atrophy of these patients.

We can also point out that MCIs of the subgroup of STN patients with a CT scan delay higher than 17 days are very close to the subgroup of GPm patients with a CT scan delay lower than 17 days. This similarity explains why the decision tree did not choose the stimulation target as predictive variable for the root node.

Another remark is the important variance on the ventricles zone observed for GPm patients when the CT scan was performed more than 17 days after surgery. This is due to the high anatomical variability of this group of patients, probably associated to high brain atrophy. Brain atrophy, indeed, causes a reduction of the ventricles, which in turns affects the electrodes curvature in this particular zone.

5. Conclusion

Since the brain can shift slightly during and after DBS surgery, there is a possibility that the implanted electrodes may also be displaced or dislodged. Several factors are likely to influence this brain shift phenomenon. In this paper, we presented results on the analysis of electrode curvature in order to better understand the brain shift phenomenon. We first proposed a method for the automatic segmentation and modelling of DBS electrode trajectories from post-operative CT images and estimated a degree of curvature for each electrode. Our hypothesis was that the degree of curvature of electrodes was deeply linked to the degree of the brain shift. We then correlated electrode curvatures of 76 patients with patients' clinical data in order to better understand the brain shift phenomenon. The CT scan delay was found to be the variable with the most influence on the degree of curvature.

Based on our results, we suggested that post-operative CT should be taken at least 2 weeks after surgery (when the potential inverse brain shift had resolved) for accurate post-operative image-based identification of electrode and contacts from CT images. Additionally, the stimulation target was also found to have a major role in studying the brain shift through electrode curvature. Disease duration, patient sex and main pathology also showed to play a role in explaining the electrode curvature data, even with a smaller impact than the other two. We found no impact on electrode MCIs for patient age, pathology form and order of electrode implantation. Finally, we conducted a local electrode curvature analysis based on these results and found that the curvature was approximately equally distributed on the entire length of electrodes. We believe that this type of analysis can contribute in improving electrode placement in DBS using further predictive mathematical models.

Acknowledgement: Authors would like to thank ANR, French National Agency of Research through the *Acoustic* project for the support of this work.

Conflict of interest: The authors declare that they have no conflict of interest.

References

[1] Benabid, AL., Krack, P., Benazzouz, A., Limousin, P., Koudsie, A., Pollak, P. Deep brain stimulation of the subthalamic nucleus for Parkinson's disease: methodologic aspects and clinical criteria. Neurology, 55:40-44 (2000)

[2] Mink, JW., Walkup, J., Frey, KA., et al. Patient selection and assessment recommendations for deep brain stimulation in Tourette syndrome. Mov Disord. 21(11), 1831-8 (2006)

[3] Lakhan, SE., Callaway, H. Deep brain stimulation for obsessive-compulsive disorder and treatment-resistant depression : systematic review. MBM research notes. 4, 3(1), 60 (2010)

[4] Biseul, M., P. Sauleau, C. Haegelen, P. Trebon, D. Drapier, S. Raoul, S. Drapier, F. Lallement, I. Rivier, Y. Lajat, and M. Verin. Fear recognition is impaired by subthalamic nucleus stimulation in parkinson's disease. Neuropsychologia, 43:1054–1059 (2005)

[5] Alegret, M., C. Junque, F. Valldeoriola, P. Vendrell, M. Pilleri, J. Rumia, and E. Tolosa. Effects of bilateral subthalamic stimulation on cognitive function in Parkinson disease. Arch Neurol, 58:1223–1227 (2001)

[6] Dujardin, K., S. Blairy, L. Defebvre, P. Krystkowiak, U. Hess, S. Blond, and A. Destee. Subthalamic nucleus stimulation induces deficits in decoding emotional facial expressions in parkinson's disease. J Neurol Neurosurg Psychiatry. 75:202–208 (2004)

[7] Saint-Cyr, L. Trepanier, R. Kumar, A. Lozano, and A. Lang. Neuropsychological consequences of chronic bilateral stimulation of the subthalamic nucleus in parkinson's disease. Brain, 123:2091–2108 (2000)

[8] Elias, KM. Fu, RC. Frysinger. Cortical and subcortical brain shift during stereotactic procedures. JNeurosurg 107:983-988, (2007)

[9] Winkler, D., Tittgemeyer, M., Schwarz, J., Preul, C., Strecker, K., Meixensberger, J. The first evaluation of brain shift during functional neurosurgery by deformation field analysis. J Neurol Neurosurg Psychiatry. 76-1161–1163 (2005)

[10] Petersen, EA., Holl, EM., Martinez-Torres, I., Foltynie, T., Limousin, P., Hariz, MI., Zrinzo, L. Minimizing brain shift in stereotactic functional neurosurgery. Neurosurgery 67:213-221 (2010)

[11] Sillay, KA., Kumbier, LM., Ross, C., Brady, M., Alexander, A., Gupta, A., Adluru, N., Miranpuri, GS., Williams, JC. Perioperative brain shift and deep brain stimulation electrode deformation analysis: implications for rigid and non-rigid devices. Annals of Biomed Eng. In press (2012)

[12] Starr, PA. Subthalamic nucleus deep brain stimulator placement using high-field interventional magnetic resonance imaging and a skull-mounted aiming device: technique and application accuracy. J Neurosurgery. 112, 479-790 (2010)

[13] Chen, I., Coffrey, AM., Ding, S., Dumpuri, P., Dawant, BM., Thompson, RC., Miga, MI. Intraoperative brain shift compensation: accounting for dural depta. IEEE TMI. 58(3), 499-508 (2011)

[14] Miga, M., Paulsen, K., Hoopes, P., Kennedy Jr., F., Hartov, A., Roberts, D.: In vivo quantification of a homogeneous brain deformation model for updating preoperative images during surgery. Biomedical Engineering 47(2), 266–273 (2000)

[15] Bucki, M., Lobos, C., Payan, Y.: Framework for a low-cost intra-operative image-guided neuronavigator including brain shift compensation. In: IEEE Engineering in Medicine and Biology Society, pp. 872–875 (2007)

[16] Clatz, O., Delingette, H., Talos, I.F., Golby, A.J., Kikinis, R., Jolesz, F.A., Ayache, N., Warfield, S.K.: Robust nonrigid

registration to capture brain shift from intra-operative MRI. IEEE Transactions on Medical Imaging 24(11), 1417–1427 (2005)
[17] Zhang, C., Wang, M., Song, Z.: A brain-deformation framework based on a linear elastic model and evaluation using clinical data. Transactions on Biomedical Engineering 58(1), 1-9 (2011)
[18] Pallavaram, S., D'Haese, PF , Remple, MS., Neimat, JS., Kao, C., Rui, Li., Konrad, PE., Dawant, BM. Detecting brain shift during deep brain stimulation surgery using intra-operative data and functional atlases: a preliminary study. ISBI. 362-365 (2009)
[19] Pallavaram, S., Dawant, BM., Remple, MS., Neimat, JS., Kao, C., Konrad, PE., D'Haese, PF. Effect of brain shift on the creation of functional atlases for deep brain stimulation surgery. Int J Comput Assist Radiol Surg. 5(3), 221- (2010)
[20] Bilger, A., Dequidt, J., Duriez, C., Cotin, S. Biomechanical simulation of electrode migration for deep brain stimulation. Int Conf Medical Image Computing Computer-Assisted Intervention. 6891, 339-346 (2011)
[21] Miyagi, Y., Shima, F., Sasaki, T. Brain shift: an error factor during implantation of deep brain stimulation electrodes. J Neurosurg, 107:989-997 (2007)
[22] Halpern, CH., Danish, SF., Baltuch, GH., Jaggi, JL. Brain shift during deep brain stimulation surgery for parkinson's disease. Stereotact Funct Neurosurg. 86(1), 37-43 (2008)
[23] Khan, MF., Mewes, K., Gross, RE., Skrinjar, O. Assessment of brain shift related to deep brain stimulation surgery. Stereotact Funct Neurosurg, 86(1), 44-23 (2008)
[24] Kim, Y.H., Kim, H.J., Kim, C., Kim, D.G., Jeon, B.S., Paek, S.H.: Comparison of electrode location between immediate postoperative day and 6 months after bilateral subthalamic nucleus stimulation. Acta Neurochir 152(12), 2037–2045 (2010)
[25] van den Munckhof, P., Contarino, MF., Bour, LJ., Speelman, JD., die Bie, RM., Schuuman, PR.. Postoperative curving and upward displacement of deep brain stimulation electrodes caused by brain shift. Neurosurgery, 67:49-53 (2010)
[26] Obuchi T, Katayama Y, Kobayashi K, Oshima H, Fukaya C, Yamamoto T. Direction and predictive factors for the shift of brain structure during deep brain stimulation electrode implantation for advanced Parkinson's disease. Neuromodulation 11:302–310 (2008)
[27] Azmi, H., Machado, A., Deogaonkar, M., Rezai, A. Intracranial air correlates with preoperative cerabral atrophy and stereotactic error during bilateral STN DBS surgery for Parkinson's disease. Sterotact Funct Neurosurg. 89(4), 246-52 (2011)
[28] Nazzaro, JM, Lyons, KE., Honea, RA., Mayo, MS., Cook-Wiens, G., Harsha, A., Burns, JM, Pahwa, R. Head positioning and risk of pneumcephalus, air embolism, and hemorrhage during subthalamic deep brain stimulation surgery. Acta Neurochir (Wien). 152, 2047-2052 (2010)
[29] Slotty, PJ., Kamp, MA., Wille, C., Kinfe, TM., Steiger, HJ., Vesper, J. The impact of brain-shift in deep-brain stimulation surgery: observation and obviation. Acta Neurochi. In press (2012)
[30] Lang, AE., Lozano. AM. Parkinson's Disease. The New England Journal of Medicine, 339: 1044-1053 (1998)
[31] Langston JW, Widner H, Goetz CG, Brooks D, Fahn S, Freeman T, Watts R. Core assessment program for intracerebral transplantation (CAPIT). Mov Dis, 1992; 7(1): 2-13.
[32] Krack P, Pollak P, Limousin P, Hoffmann D, Xie J, Benazzouz A, Benabid AL. Subthalamic nucleus or internal pallidal stimulation in Young onset Parkinson's disease. Brain, 1998; 121: 451-7.
[33] Coupe, P. Yger, S. Prima, P. Hellier, C. Kervrann, and C. Barillot. An optimized blockwise nonlocal means denoising filter for 3-D magnetic resonance images. IEEE TMI. 24:425-441 (2008)
[34] Powell, M. The NEWUOA Software for Unconstrained Optimization without Derivatives", Workshop On Large Scale Nonlinear Optimization, G. Di Pillo and M. Roma, eds., Nonconvex Optimization and Its Applications 83, Springer (2004)
[35] Seber, GAF. and Wild, CJ. Nonlinear regression. New York: John Wiley and Sons (1989)
[36] Lalys, F., Haegelen, C., Mehri, M., Drapier, S., Vérin, M., Jannin, P. Anatomoc-clinical atlases correlate clinical data and electrode contact coordinates : application to subthalamic deep brain stimulation. J Neursocience methods (E-pub ahead of print)
[37] Gray, A., Abbena, E., Salamon, S. Modern differential geometry of curves and surfaces with mathematica. The Gaussian and Mean Curvatures. Boca Raton, 2nd ed.:373–380 (1997)
[38] Breiman, L., Friedman, J., Olshen, R., Stone, C. CART: Classification and Regession Trees. Wadsworth International (1984)
[39] Haegelen C., Coupe P., Fonov V., Guizard N., Jannin P., Morandi X., Collins DL. Automated segmentation of basal ganglia and deep brain structures in MRI of Parkinson's Disease, IJCARS (2012)